A stochastic upscaling approach of impregnation flows in fibrous microstructures for composite process modelling

Sylvain Drapier, Aubin Geoffre, Nicolas Moulin, Julien Bruchon

A STOCHASTIC UPSCALING APPROACH OF IMPREGNATION FLOWS IN FIBROUS MICROSTRUCTURES FOR COMPOSITE PROCESS MODELLING

S. Drapier[1], A. Geoffre[2], N. Moulin[1] and J. Bruchon[1]

[1]SMS & LGF UMR CNRS 5307, Mines Saint-Etienne
158, Cours Fauriel 42100 Saint-Etienne, France
Email: {drapier, nmoulin, bruchon}@emse.fr, https://www.mines-stetienne.fr/en/author/drapier/
[2]CMAT UMR CNRS 7633, Mines Paris – PSL, 63-65 rue Henri-Auguste Desbrueres BP 87
91003 Évry cedex, France
Email: aubin.geoffre@minesparis.psl.eu

Keywords: transient flow, fibre-scale, scale transition, microstructure, impregnation, processing

Abstract
Direct elaboration processes of composite materials, such as *LCM*, involve transient two-phase flows within multi-scale fibrous media. Based on stabilised finite element simulations of such flows at the fibre scale, statistical descriptions of the impregnation in randomly generated representative volume elements are proposed. For modelling resin infusion at the preform scale, homogenised properties are identified in both saturated and transient regimes, with assessment of the influence of boundary conditions and flow regimes on the flow dynamics in both fully and partially saturated regimes. An explicit stochastic permeability is first proposed for stationary regimes. Then, capillary pressures and local saturation dynamics are identified for transient two-phase flows with surface tension effects. Eventually, identification of the length-scales at play which have never been established so far leads to draw some limits on the validity of homogenization process, depending on both geometry and physics.

1. Introduction

Out-of-autoclave direct elaboration processes stand now as very attractive alternatives to dry routes processes (pre-impregnated) for manufacturing structural materials with significant energy and economic gains – Figure 1. This work concerns more particularly the infusion processes in which dry preforms, made up of architectured long fibres reinforcement, are laid on a half-mold before being impregnated by a liquid resin under the action of a vacuum.

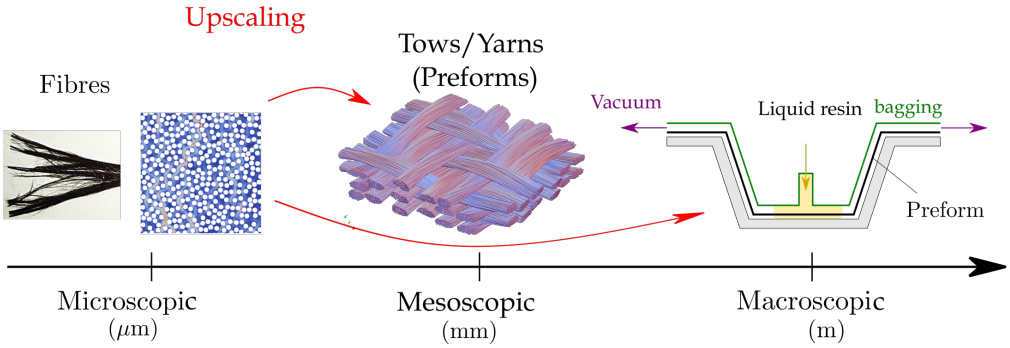

Figure 1. Scales of observation and flows in infusion-based processes

Usually, the impregnation stage is modelled through simulations at the part scale but involving somehow complex ‘material parameters’ carrying more and more fine descriptions to try and approach reality. Indeed, the industrial part can reach several meters, while it consists of fibres of only a few microns in

diameter - Figure 1. Obviously, this rises lots of questions about the upscaling of local information obtained at the fibre scale, potentially stochastic, to larger scales, *i.e.* the homogenisation methods that can be applied for upscaling saturated as well as partially saturated flows. In a more global view, one can see impregnation as a transient two-phase flow within a geometrically complex and multi-scale fibrous medium.
This work encompasses both flow regimes that can be met in infusion-based processes. Computations are carried out, within a stabilised Finite Element framework, on validated Representative Volume Element (RVEs) and averaged over the volume in order to establish a probabilistic response that can be used at upper scales. First is presented the case of a permanent single-phase flow [1]. In this framework, the notion of permeability introduced in the Darcy's law is generally sufficient to characterise the scale-up [2]. Through a statistical study of dimensionless randomly generated RVEs, the factors controlling these local flows are identified. A versatile explicit stochastic permeability is then proposed which includes the most significant morphological descriptors, along with the effect of fluid/fibre contact slip. Then, keeping a similar statistical approach, a more realistic situation with respect to the process is studied, in which the liquid resin drives out the air initially contained in the medium. Modeling such a transient two-phase flow at the microscopic scale requires absolutely to consider the capillary effects originating from the surface tensions acting at the fibre-fluid-air interface. During transient flows, these capillary effects are in competition with the viscous effects. This greatly controls the observed flow [3] in terms of saturation dynamics, preferential flow paths, residual porosities, ...

2. Materials and methods

2.1. Modelling saturated and transient flows

In accordance with the regime met in *LCM* processes, fluid flows are modelled here in laminar regime through the Stokes' equations ($\nabla \cdot v = 0$ and $\mu \Delta v - \nabla p = 0$) complemented by Dirichlet's and Neuman's boundary conditions, with v the fluid velocity, p the fluid pressure and μ the fluid viscosity. A complementary condition can be introduced which models the contact between both fluid and solid phases. The so-called Navier's slip condition [4] is prescribed on the liquid/solid interface Γ_{LS}, it relates the fluid tangential velocity to the shear components of the fluid Cauchy stress tensor $\boldsymbol{\sigma}$ through a slip length ℓ_s [5] and reads (Figure 2):

$$\mathbf{v} \cdot \mathbf{t} = -(\ell_S / \mu_L)\, \mathbf{t} \cdot \boldsymbol{\sigma} \cdot \mathbf{n} \quad \text{on } \Gamma_{LS} \tag{1}$$

where $\mathbf{t}$ (resp. $\mathbf{n}$) is a unit tangential (resp. normal) vector to Γ_{LS}. This generalises no-slip ($\ell_s \to 0$) and free-slip conditions ($\ell_s \to \infty$). It will be shown that this condition has a large influence on the flow. In saturated regime, knowing the fluid velocity and pressure fields computed, the solution is then upscaled to extract permeability from the Darcy's law [2]:

$$\mathbf{v}_D = -(\mathbf{K} / \mu) \cdot \nabla p_D \tag{2}$$

where $\mathbf{v}_D$ (resp. p_D) is the upscaled velocity (resp. pressure) and $\mathbf{K}$ the second order permeability tensor. This upscaling procedure must be performed on RVEs that are the smallest geometry for which permeability, and other associated characteristics, become independent of the domain size [1, 6].

For transient regimes, schematically depicted in Figure 2, the physics to be modelled is more complex, it implies two phase-flows in the poral structure. These fluids are named here as vapor (or air) and liquid, defined respectively by their viscosity: μ_V and μ_L. Moreover, surface tension effects must be accounted for in two ways so that capillary effects are properly represented since they can reach up to 1/3 of the driving pressure in infusion-based processes [5, 7]. First, due to the presence of 3 phases - liquid, fluid, and solid- at triple points (lines in 3D) menisci will form to enforce surface tension equilibrium (Eq. 3a). Second, the liquid-vapor interface will experience this surface tension equilibrium also, accounted for through the Laplace's law (Eq. 2) [5] which relates the normal stress vector jump $[[\boldsymbol{\sigma} \cdot \mathbf{n}]]_I$ at interface

j to the mean curvature $\mathscr{C}$ of this interface (Eq. 3b). These 2 conditions introduce interfacial discontinuities which translate into some driving forces usually referred to as wicking force and capillary pressure. They summarise as:

$$\gamma_{LS}\,\mathbf{t}_{LS} + \gamma_{LV}\,\mathbf{t}_{LV} + \gamma_{SV}\,\mathbf{t}_{SV} = 0 \qquad \text{at } \Gamma_{LS} \cap \Gamma_{LV} \cap \Gamma_{SV} \qquad \text{(3-a)}$$

$$[[\boldsymbol{\sigma} \cdot \mathbf{n}]]_{LV} = -\,\gamma_{LV}\,\mathscr{C}\mathbf{n} \qquad \text{on } \Gamma_{LV} \qquad \text{(3-b)}$$

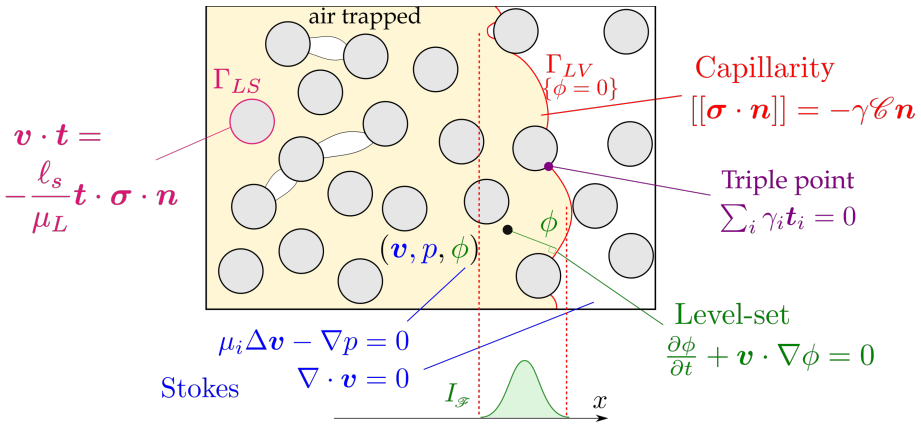

Figure 2. Schematic of transient flow description.

Let us finally remark that the saturated regime may be seen as a particular case of the transient regime: 'sufficiently' behind the flow front, a steady quasi-saturated regime will be reached. One can anticipate that a proper representation of transient flows in 'sufficiently' large RVEs may permit to characterise transient and steady flows, and hence both responses of the medium with highly reduced CPU efforts.

2.2. Numerical modelling approach

Before concentrating on the flow characterisation, the numerical framework used for solving this problem numerically has to be recalled briefly; all the details can be found in the publications of our group, for instance [5, 8] … In few words, Stokes' flows (liquid and vapor) are solved in a monolithic approach, using the same mixed velocity-pressure P1/P1 finite elements stabilised by an *Algebraic SubGrid Scal*e method. The Navier's condition is implemented in this FE approach [1] along with the weak enforcement of the surface tension equilibria (Eqs 3-a and 3-b) as described in [5]. For transient flows, the *Level-set* method [6] has been selected for its numerous capabilities, and under the constraint of applying as precisely as possible some conditions on interfaces such as the surface tension effects described above that depend on the interface curvature (Eq. 3b). Basically, this method consists in defining a scalar field ϕ, usually the signed distance to the interface -Figure 2 -, and describe the interface as the 0 iso-value of this level-set. This field is convected in a velocity field, here the computed fluid velocity, through the same linear FE scheme but stabilised with a SUPG method [5]. A staggered weak coupling is considered, where fluid velocity is computed on a fixed domain and then used to update the flow front position and properties. All these methods are implemented in a robust environment validated on lots of test cases along the past and recent years [1, 5, 8, …], in the finite element code Zset[1].
Eventually, the RVEs are to be provided for these simulations. A specific generation scheme has been developed [1] which permits to generate random RVEs with periodic boundaries, statistically representative of the fibre distribution that can be actually measured in long fibre micro-structures [7]. Given variable fibre radii following a normal distribution, typically $r = \mathcal{N}(\bar{r}, 0.1\bar{r})$, ($\bar{r}$ is the mean fibre radius) and a target fibre fraction, microstructures are generated and optimal finite element meshes are produced that ensure a proper description of the fluid flow together with minimum number of elements - *see* Figure 3.

[1] http://www.zset-software.com/

For the simulations, typical materials have been considered: mean fibre radius $\bar{r}$ =3.5 µm, resin as liquid and air as vapor, fibre volume fractions (V_f the volume of fibre over the total volume) from 0.3 to 0.65. The corresponding material data are given in Table 1.

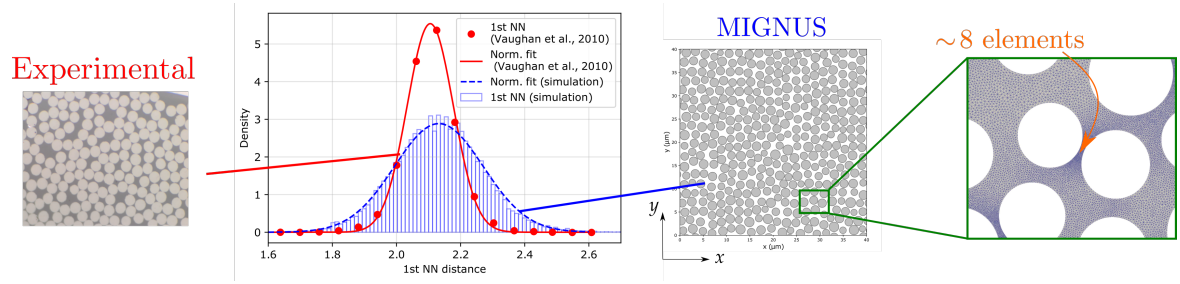

Figure 3. MIGNUS scheme for the generation of random SRVEs - statistically representative volume element- and associated finite element mesh [1].

Table 1. Material data : viscosity μ_i and surface tension γ_{ij}.

μ_L (Pa.s)	μ_V (Pa.s)	γ_{LS} (N.m^{-1})	γ_{SV} (N.m^{-1})	γ_{LV} (N.m^{-1})
2.76 x 10^{-3}	1.71 x 10^{-5}	54.7 x 10^{-3}	25.9 x 10^{-3}	50.8 x 10^{-3}

2.3. Scale transition – upscaling methods

Saturated cases consist typically in applying a pressure gradient in a direction (***x*** or ***y*** in Figure 3) and measuring the fluid velocity (flux) across the boundaries in both directions to identify the corresponding permeability tensor components – tensor not necessarily diagonal nor symmetric [8] - through the Darcy's law (Eq. 2). For the flows in transient regimes, the upscaling procedure is not so standard, and the first questioning comes about the relevant physically-sound characteristics that can be upscaled. Looking at literature, in composite materials [3, 7, 11, 12] but also in hydrogeology for instance [8], transient permeabilities may be extracted from transient flows but overall the question is : " is it relevant to estimate a transient permeability to feed infusion simulations at the upper scale ? " Indeed, we do believe that other local descriptors may be more relevant for transient flows provided statistical RVE can be defined; these may be the equivalent capillary pressure acting overall on the fluid front, or some more informative characteristics such as saturation in the RVE or other descriptors of the flow front. In both regimes, Gaussian Regression Processes (GPR) / Machine learning is considered to capture the inherent stochastic character of the physics in play.

As stated previously, a normal capillary stress discontinuity (Eq. 3-a) appears at the liquid-vapor interface. In a homogenisation context, the overall contribution P_{cap} can characterise the capillary action at an upper scale [13, 14]. Two methods can be considered to evaluate the averaged capillary pressure (Eq. 5): measure directly the average pressure drop at the liquid-vapor interface Γ_{LV} [9], and estimate the normal stress from the interface curvature (Laplace's law, Eq. 3-b [6, 14]) :

$$P_{cap} = \langle |p_L - p_V| \rangle_{\Gamma_{LV}} \qquad P_{cap} = \gamma_{LV} \langle \mathscr{C} \rangle_{\Gamma_{LV}} \tag{5}$$

where $\langle \square \rangle_{\Gamma_{LV}} = \frac{1}{|\Gamma_{LV}|} \int_{\Gamma_{LV}} \square dS$ is the surface average over Γ_{LV}.

Another key feature of transient flows in porous media is the saturation which represents the ratio between the volume of fluid and the total poral space ($S_L \in [0,1]$). This information can be local, for a given section along the flow, or global. Let us note that for saturation as well as P_{cap}, the liquid-vapor interface must be carefully processed to extract the non-contiguous interface pieces of the moving flow front, disregarding the 'bubbles' trapped in the fibre network, downwards the flow – *see* Figure 2 for illustration of the concept and [13] for details.

3. Results

3.1 Saturated flows

For selected fibre volume fractions ranging from 0.3 to 0.6, some sets of 150 microstructures were generated using the MIGNUS procedure (Figure 3) and studied; all the details can be found in Geoffre *et al.* [1]. The optimum RVE size was shown to depend directly on the fibre volume fraction: the higher the volume fraction, the smaller the RVE size; if V_f varies from 0.3 → 0.6, $\ell_{RVE}/\bar{r}$ varies from 100 → 60. A statistical study demonstrated that:

- the permeability tensor is symmetric, isotropic, and follows a normal distribution for proper RVEs
- among the various morpho-mathematical descriptors, the fibre volume fraction carries 95% of the statistical information on its own - Figure 4-a
- permeabilities computed are consistent with literature models - Figure 4-a
- variability of the microstructure induced by both fibre radius variability and randomness of fibre placements yields only 3% of permeability variability - Figure 4-a.

Second, other physical parameters were considered. The most relevant effect comes from the slip length which represents the fibre-fluid 'contact': between the extreme bounds corresponding to no-slip and slip conditions the permeability may vary by a decade - Figure 4-b. Let us recall that theoretically upscaling local Stokes' flow in fibrous arrangements to Darcy's flow requires to assume a no-slip condition of the fluid [5]. From these results an explicit stochastic expression bounding the saturated permeability has been proposed, it is composed of 2 terms: one related to the intrinsic variability induced by radius and generation variability, and a second one related to the slip length :

$$K(V_f, \bar{r}, \ell_s) = \bar{r}^2\, \mathcal{N}(1, 3\%)\, e^{1.18(1-10V_f)} \left[1 - \frac{1-e^{-3.86V_f}}{1+\frac{1}{2}\frac{\bar{r}}{\ell_S}}\right] \tag{6}$$

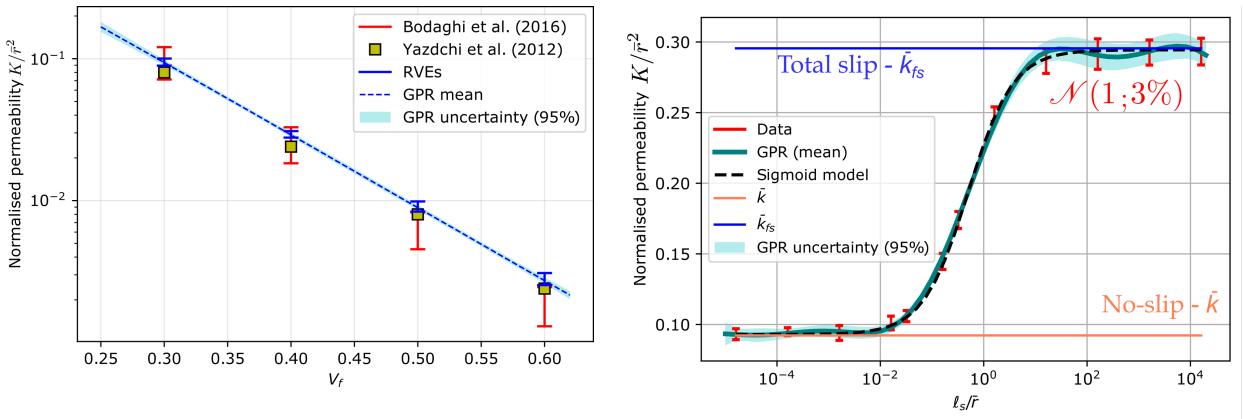

(a) (b)

Figure 4. Saturated stochastic normalised permeability results [1]: (a) comparison with literature, and (b) as a function of the normalised slip length $\ell_S/\bar{r}$ for $V_f = 0.3$ (30 RVEs at every $\ell_S/\bar{r}$).

Syerko *et al.* [10] published in 2023 the results of a Virtual Permeability benchmark. Let us compare the predictions of our analytical model [1] with some of these results finally deemed representative of transverse in-plane saturated permeabilities (Figure 22 in [10]). In Figure 5, one can verify that our stochastic permeability compares well with the results from heavy computations relying on tedious image post-processing. For illustration are also reported the predictions from the very simple but useful analytical Gebart's model [11] established for periodic arrangements (Square / Hexa packings). In light of the results from RVE size determination ($\ell_{RVE}/\bar{r} \gtrsim 80$), K_{xx} (isotropy plane (O, ***x***, ***z***) in [10]) can be trusted, with some tens of fibres in the flow direction (1 mm long, and $\bar{r}$ = 4.2 µm), while K_{zz} is questionable, like stated in [10], since only few fibres are present in this direction (0.125 mm long ⇔ 20 $\bar{r}$, *see* Figures 9 and 15-a in [10]) and fibre volume fractions range from 0.54 to 0.59 (*see* Figure 5).

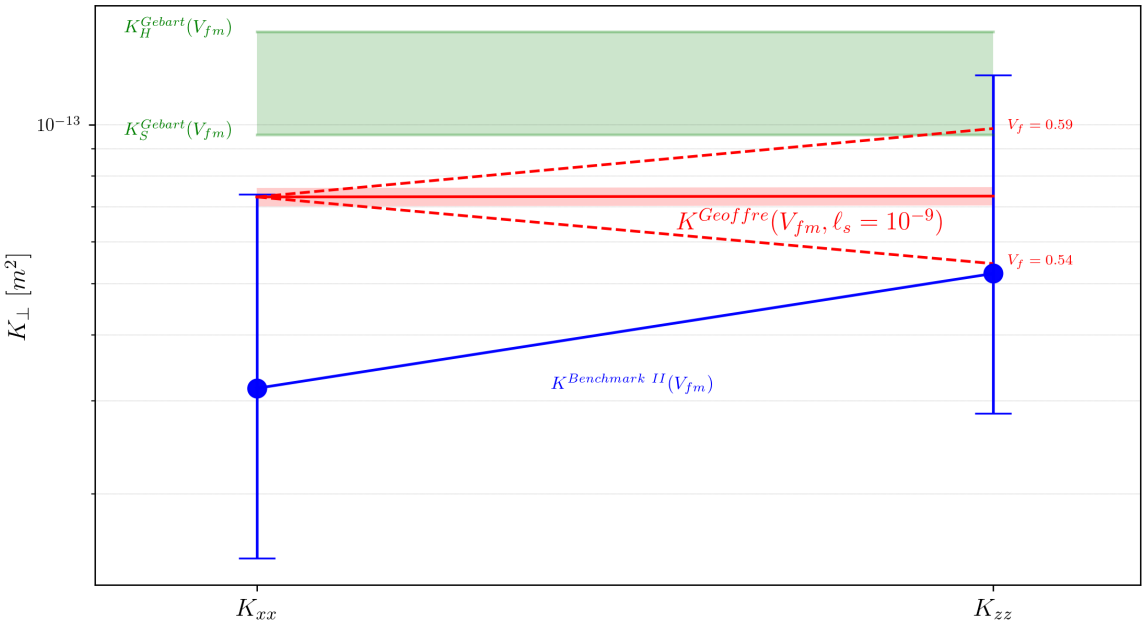

Figure 5. Comparison of saturated permeabilities from Gebarts's [11] and Geoffre's models (with sticking conditions) with results from the virtual permeability benchmark [10]; mean fibre fraction V_{fm}=0.565.

3.2 Transient regime

Simulations were carried out in transient regime on the same RVEs, optimised in terms of computation costs and representativity, with a size $\ell_{RVE}/\bar{r} = 40$ sufficient to define a Statistical RVE. As commonly admitted, the flow is characterised by its capillary number [3, 6], the ratio of viscous effects to the surface tension effects : $Ca = \mu_L \|\bar{v}\| / \gamma_{LV}$ with $\bar{v}$ is the fluid inlet velocity that is prescribed in our case.

Computations reveal the dynamics of infusion and permits to verify that the RVE size is sufficient, *i.e.* a large part of the RVE can be filled before the flow front reaches the outlet. The overall saturation depends on *Ca* (Figure 6) but not significantly on the fibre fraction. Additionnally, for our material configurations the saturation 'front' width is measured at $\ell_{sat} \approx 8\,\bar{r}$.

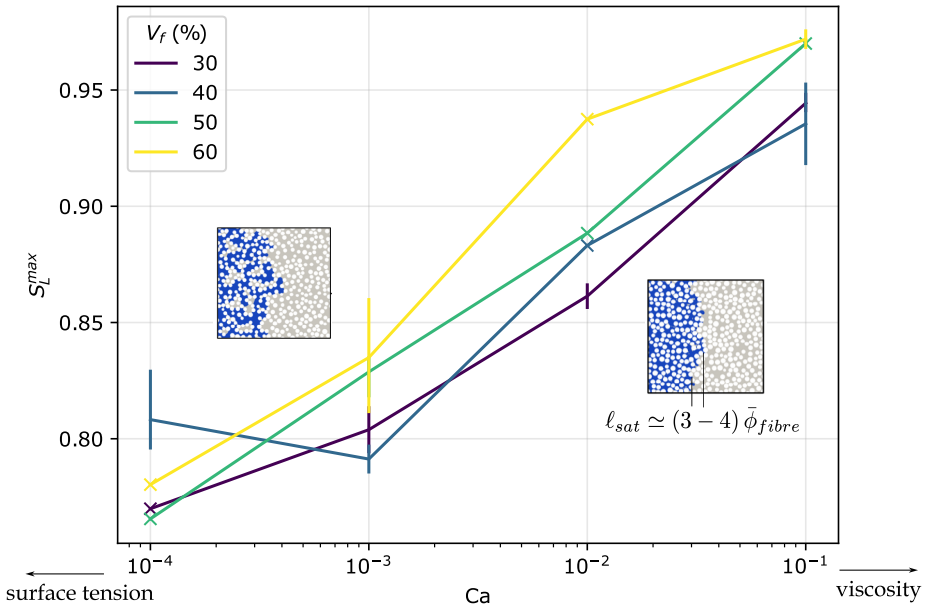

Figure 6. Saturation as a function of the capillary number *Ca*, for fibre fractions V_f from 30 to 60%.

Moreover, the capillary pressure estimated through both methods (Eqs. 5) appear to be similar. Direct comparisons with the very few experimental measurements are to be considered with care since flow regimes are not directly provided. In Figure 7, one can verify that the computed results correspond to an extension of the Ahn's analytical model [14] with a known non-linear dependance upon the fibre fraction, but more importantly function of the flow type, especially for viscosity driven flows ($Ca \gtrsim 10^{-3}$-10^{-2}). Let us note that by varying viscosities and surface tensions, Ca was shown to characterize flows on its own, in the range $Ca \in [10^{-4}\text{-}10^{-1}]$.

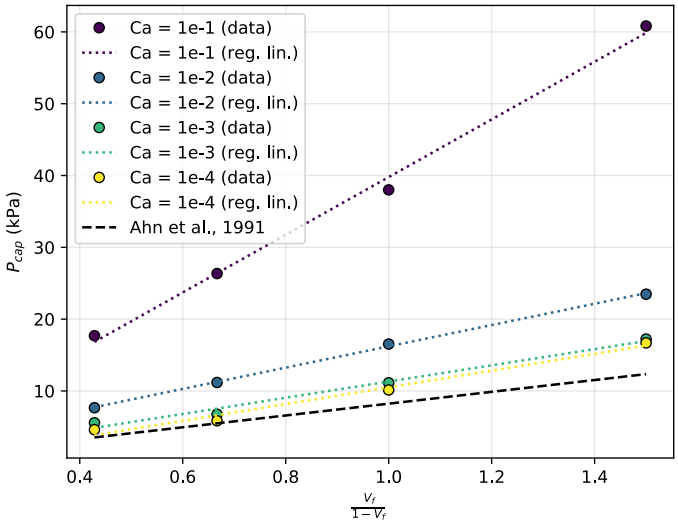

Figure 7. Capillary pressure as a function of the fibre fractions for Vf from 30 to 60% : analytical from [14] and computed for capillary numbers *Ca* from 10^{-4} to 10^{-1} [13].

Eventually, knowing the saturation length ($\ell_{sat} \approx 8\,\bar{r}$), and global saturation dynamics, one can estimate whether a full description of the flow can be properly represented using a simple Darcy's approach, knowing the identified permeability (Eq. 6). We have shown that, provided the medium is sufficiently large, *i.e.* $\ell_{RVE} >> \ell_{sat}$, this simplification holds for flows with $Ca \gtrsim 10^{-2}$ corresponding to 'well' saturated VER ($S_L \gtrsim 85\%$ and pictures in Figure 6). In that case the error, measured for instance as the inlet pressure difference for both full and simplified representations, is lower than 10% (Figure 8) .

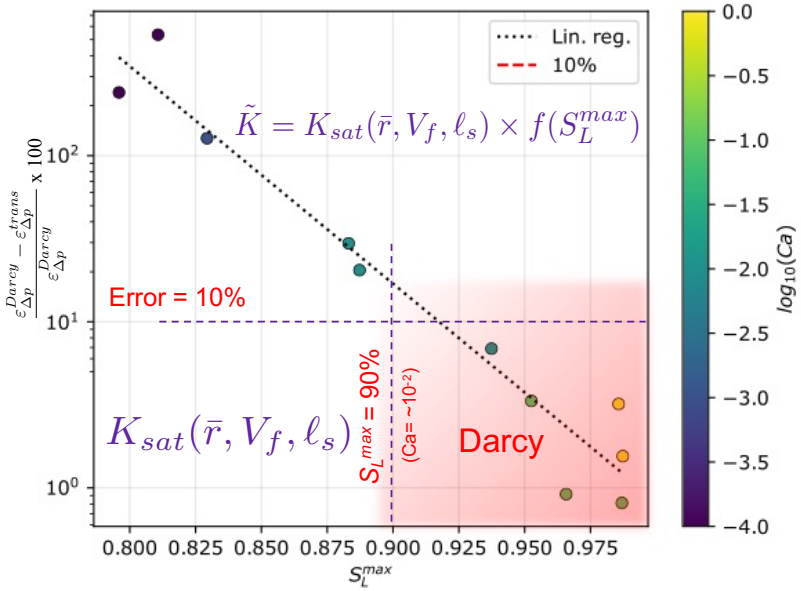

Figure 8. Difference in inlet pressure (velocity prescribed) between Darcy's type or fully described flow, depending on Ca and for $V_f = 0.5$. 10% admissible difference corresponds to $Ca \gtrsim 10^{-2}$.

5. Conclusions

Relying on very robust simulation capabilities and well-grounded upscaling statistical approaches, we have explored the infusion of resin in long-fibre composite microstuctures. Numerous computations carried out on various RVEs have permitted to optimise the RVE size in saturated regime, and propose an explicit stochastic relation between permeability and fibre volume fraction, but which accounts in the meantime for the resin-fibre affinity as well as the micro-structure variability induced by both fibre radius and RVE randomness – *see* [1]. Comparisons with some results computed from CT-images, reported in an international benchmark, yield positive conclusions. Second, transient flows have been considered, incorporating all the surface tension effects which largely control these flows. In that case, the most relevant descriptor of the flow appear to be the global saturation that depends on the type of flow but not on the fibre volume fraction. Also, capillary pressure was consistently estimated through 2 methods, the results of which are in accordance with literature and provide an explicit extension of some simplified models for diverse flow types. Eventually, the local saturation, newly established ($\ell_{sat} \approx 8\,\bar{r}$ for Ca $\in [10^{-4}\text{-}10^{-1}]$), is a precious indicator that canl measure the scales separation: the saturation length permits to wisely build homogeneous equivalent media for upscaled flows and quantify this simplification.

REFERENCES

[1] A. Geoffre, M. Ghestin, N. Moulin, J. Bruchon, and S. Drapier, “Bounding transverse permeability of fibrous media: a statistical study from random representative volume elements with consideration of fluid slip,” *International Journal of Multiphase Flow*, vol. 143, p. 103751, 2021.
[2] H. Darcy, *Les fontaines publiques de la ville de Dijon*. Dalmont, 1856.
[3] V. Michaud, “A Review of Non-saturated Resin Flow in Liquid Composite Moulding processes,” *Transp Porous Media*, vol. 115, no. 3, pp. 581–601, 2016.
[4] V. Rougier, J. Cellier, M. Gomina, and J. Bréard, “Slip transition in dynamic wetting for a generalized Navier boundary condition,” *J Colloid Interface Sci*, vol. 583, pp. 448–458, 2021.
[5] L. Chevalier, J. Bruchon, N. Moulin, P. J. Liotier, and S. Drapier, “Accounting for local capillary effects in two-phase flows with relaxed surface tension formulation in enriched finite elements,” *Comptes Rendus - Mecanique*, vol. 346, no. 8, pp. 617–633, 2018.
[6] M. Sussman, P. Smereka, and S. Osher, “A Level Set Approach for Computing Solutions to Incompressible Two-Phase Flow,” *J Comput Phys*, vol. 114, no. 1, pp. 146–159, 1994.
[7] T. J. Vaughan and C. T. McCarthy, “A combined experimental-numerical approach for generating statistically equivalent fibre distributions for high strength laminated composite materials,” *Compos Sci Technol*, vol. 70, no. 2, pp. 291–297, 2010.
[8] S. Whitaker, “Flow in porous media I: A theoretical derivation of Darcy’s law,” *Transp Porous Media*, vol. 1, no. 1, pp. 3–25, 1986, doi: 10.1007/BF01036523.
[9] S. Konangi, N. K. Palakurthi, N. K. Karadimitriou, K. Comer, and U. Ghia, “Comparison of pore-scale capillary pressure to macroscale capillary pressure using direct numerical simulations of drainage under dynamic and quasi-static conditions,” *Adv Water Resour*, vol. 147, no. December 2019, 2021, doi: 10.1016/j.advwatres.2020.103792.
[10] E. Syerko *et al.*, “Benchmark exercise on image-based permeability determination of engineering textiles: Microscale predictions,” *Compos Part A Appl Sci Manuf*, vol. 167, no. August 2022, 2023.
[11] B. R. Gebart, “Permeability of Unidirectional Reinforcements for RTM,” *J Compos Mater*, vol. 26, no. 8, pp. 1100–1133, 1992, doi: 10.1177/002199839202600802.
[12] M. F. Pucci, P. J. Liotier, and S. Drapier, “Capillary wicking in a fibrous reinforcement - Orthotropic issues to determine the capillary pressure components,” *Compos Part A Appl Sci Manuf*, vol. 77, pp. 133–141, 2015, doi: 10.1016/j.compositesa.2015.05.031.
[13] A. Geoffre, N. Moulin, J. Bruchon, and S. Drapier, “Reappraisal of Upscaling Descriptors for Transient Two-Phase Flows in Fibrous Media,” *Transp Porous Media*, no. 0123456789, 2023.
[14] K. Ahn, J. Seferis, and J. Berg, “Simultaneous measurements of permeability and capillary pressure of thermosetting matrices in woven fabric reinforcements,” *Polymer composites*, vol. 12, no. 3, pp. 146–152, 1991.